Reaction mechanism of low-temperature catalysis by surface protonics in an electric field

Journal:	*Faraday Discussions*
Manuscript ID	FD-ART-12-2019-000129.R1
Article Type:	Paper
Date Submitted by the Author:	24-Dec-2019
Complete List of Authors:	Sekine, Yasushi; Waseda University, Applied Chemistry Manabe, Ryo; Waseda University, Applied Chemistry

SCHOLARONE™
Manuscripts

Reaction mechanism of low-temperature catalysis by surface protonics in an electric field

Yasushi Sekine*[a], Ryo Manabe[a]

The process combining heterogeneous catalysts and DC electric field can achieve high catalytic activities, even under mild conditions (<500 K) with less electrical energy consumption. Hydrogen production by steam reforming of methane, aromatics and alcohol, dehydrogenation of methylcyclohexane, dry reforming of methane, and ammonia synthesis are known to proceed at low temperatures in an electric field. *In-situ/operando* analyses have been conducted using IR, Raman, XAFS, electrochemical impedance spectroscopy, and isotopic kinetic analyses to elucidate the reaction mechanism for these reactions at low temperatures. Results show that surface proton hopping by a DC electric field, called surface protonics, is important for these reactions at low temperatures because of higher surface adsorbate concentrations at lower temperatures.

Introduction

Importance of low-temperature catalysis

Many chemical processes including petroleum refining, exhaust gas cleaning, and petrochemical production use catalysis, especially heterogeneous catalysis. Commonly, the rate of heterogeneous catalysis is controlled by the Arrhenius kinetic law, i.e. $\ln k = \ln A - E_a/RT$. If the pre-exponential (frequency) factor A and the apparent activation energy E_a are fixed, then the kinetic constant k is determined by the temperature. Therefore, catalytic reactions must be operated at higher temperatures to promote a reaction. For endothermic reactions such as steam reforming and dry reforming, not only kinetic limitations but also thermodynamic equilibrium limitations should be considered when seeking higher product yields. From these viewpoints, novel catalytic systems that support catalysis at lower temperatures with higher productivity are highly anticipated.

Various processes to date for low-temperature catalysis

To date, various processes have been proposed for lowering reaction temperatures of catalysis. Fig. 1 presents a summary of various catalytic processes for low-temperature reactions. Many researchers have proposed and investigated photocatalysis, plasma-catalysis, electrocatalysis, sono-catalysis, mechano-catalysis, and bio-catalysis.
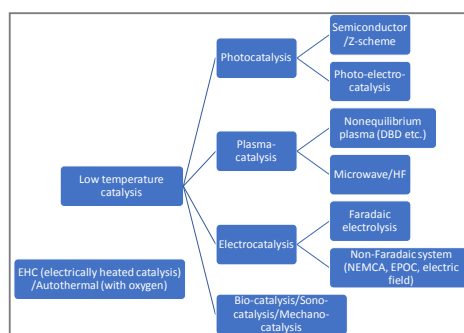
Figure 1. Various catalytic processes that work at lower temperatures.

Among them, photocatalysis is a promising option for lowering reaction temperatures. Based on findings reported by Fujishima and Honda, various semiconductor materials have been investigated for photocatalysis. Recently, a Z-scheme type system, plasmon catalysis, and other promising methods have been proposed.

Discharge and plasma technologies are sometimes combined with catalysis because electrons with high energy can activate the raw material directly in gas phase or promote active species production on the catalyst. On non-equilibrium plasma such as spark discharge [1–8] and corona discharge, [9–11] only the electron temperature increases by control of the plasma generation. The application of discharge/plasma to catalysis lowers the reaction temperature for various catalytic reactions.

As for the electrochemical routes, the impressed electron (current) is used stoichiometrically. In contrast to Faradaic reaction, some types of reactions proceeding beyond the stoichiometry of impressed electrons are reported. One is the non-Faradaic electrochemical modification of catalytic activity (NEMCA)[12,13] which is observed at higher temperature than 900

K, and another is electrochemical promotion on catalysis (EPOC) which is observed even at lower temperature range, but Faradaic in some cases [14,15]. For these two cases, a solid electrolyte is used between two electrodes, and weak current are imposed to the catalyst. These have been applied for catalysis such as ethylene oxidation [12], steam reforming of methane [16–18], methane oxidation [19], ammonia synthesis [20–22], and C2 production [23]. For steam reforming of methane, Ni film [16], Ni-YSZ cermet anode [16], Pt-YSZ-Na-βAl$_2$O$_3$ [17], and Pt-YSZ-Au [18] have been used as catalysts. The reaction proceeds 25 times faster than the number of impressed electrons with small energy consumption of 16 MJ/kg$_{-H2}$ at temperatures below 1103 K.[16] When Pt catalyst was used, the reaction proceeded at 773 K with 2 V, with nearly 50% initial conversion. The auto-thermal reforming condition (CH$_4$ + H$_2$O + O$_2$) was found to be the most appropriate and efficient for this system.[17,18] The NEMCA effect evolved into various catalyses for reasons that remain unclear. One possibility is that applied voltage/current produces an active ion species, such as oxide anions, because of changes in the work function of the catalyst.[24]

Current issues

Activation of stable molecules such as methane, nitrogen, and carbon dioxide is important because of their abundance, and for future development of sustainable energy/chemicals systems. Methane activation is among the most difficult reactions because it has very stable structure. Industrial methane conversion is limited to steam reforming of methane for hydrogen production. This reaction is conducted at very high temperatures of around 1000 K using Ni catalyst supported on Al$_2$O$_3$.[25] Because of its high reaction temperatures, carbon deposition would proceed to some degree. Also, decoking operations are required. Coking causes covering of active sites on the catalyst, consequently deactivating the catalyst.

Ammonia synthesis is conducted over various catalysts at high temperatures and pressures in terms of the limitations of kinetics and thermodynamic equilibrium. The Haber–Bosch process, which is well known as an industrial ammonia synthesis process, is operated at around 723–773 K and 200 atm, in very harsh conditions. The origin of the catalyst for ammonia synthesis is an iron catalyst discovered by Mittasch.[26] This catalyst was developed further toward an iron-based double promotion catalyst (Fe$_3$O$_4$ + Al$_2$O$_3$ and K$_2$O), where iron plays a role of adsorption and as an active site for nitrogen. It is also indicated that Al$_2$O$_3$ suppresses the sintering of iron during reduction of the catalyst, and indicated that dispersed K$_2$O promotes surface activity on iron.[27] In 1972, Aika et al. reported a supported Ru catalyst [28] that showed high activity, even at low temperatures, compared to Fe catalyst. Results suggest that hydrogen adsorption strongly influenced the Ru catalyst.

To lower these reaction temperatures, some reaction processes have been proposed as described above. For photocatalysis and NEMCA, the reaction rates are limited; large-scale production is difficult. Plasma utilization requires much energy.

Heterogeneous catalysis in an electric field

Recently, various heterogeneous reaction have been found to proceed with the aid of a DC electric field, even at low temperatures (<500 K).[29–46] Various metal-supported catalysts including Pd, Pt, Ru, Ni, and Co supported on a semiconductor support (CeO$_2$, perovskites, etc.) are useful for these systems. Direct current (DC) of several milliamperes is applied to the catalyst bed with two electrodes: a high-voltage and ground electrode (Fig. 2). Results show that several hundred volts are applied to the catalyst bed. That order of voltage is higher than that of a NEMCA system and electrolysis, but lower than that of a discharge process.

This method can be applied widely to various catalytic processes: degradation of ethanol [30], steam reforming of methane [29], aromatics [40], DME [45], or ethanol [29], water–gas shift reaction [33], dry reforming of methane [35], ammonia synthesis [46], dehydrogenation of methylcyclohexane [41–43], carbon dioxide activation (CCU) [44], and so on. Using this system, for which a schematic image is shown in Fig. 2, very high one-pass yield and conversion are obtainable even at temperatures below 500 K. A salient advantage of this process is that the rapid operation can be achieved merely by application of DC electric field at low temperatures. Therefore, this process might provide new avenues for developing small-scale and on-demand catalytic processes at low temperatures. This process is different from electric discharge, plasma, electrolysis and electrolytic reaction, and has higher energy efficiency than these. Semiconductor catalyst support is required, and surface ion hopping plays an important role on this process. Using various characterization including in-situ/operando IR/Raman/XAFS, kinetics, isotopic transient tests, and electrochemical impedance measurements, we have investigated reasons why the DC electric field application to the heterogeneous catalyst supported on semiconductor proceeds even at such low temperatures. Results revealed that surface protonic transport, "surface protonics", plays an important role in these low-temperature catalyses. As described in this paper, we can summarize the reaction mechanisms of heterogeneous catalysis using surface protonics at low temperatures.
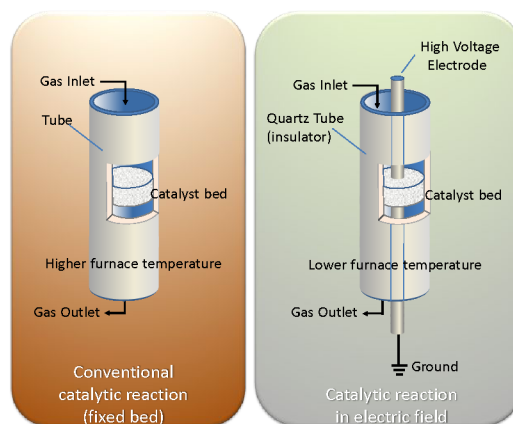

Figure 2 Schematic images of a conventional heterogeneous catalytic reaction (left) and a one in an electric field (right).

Experiment Procedure

Sample preparation

For this study, various semiconductors including CeO_2 (JRC-CEO-1 for steam reforming and MCH dehydrogenation), $SrZrO_3$ perovskite (for ammonia synthesis) were used as the catalyst support. Using an impregnation method, Pd (for steam reforming), Pt (for MCH dehydrogenation), Ru (for ammonia synthesis) or other active metal supported catalyst was prepared. For loading Pd, $Pd(OCOCH_3)$ (Kanto Chemical Co. Inc.) was used as a metal precursor, for Pt, $Pt(NH_3)_4(NO_3)_2$ (Sigma-Aldrich Corp.) was used and for Ru, $RuCl_3 \cdot 3H_2O$ (Kanto Chemical Co. Inc.) was used. The dried sample was calcined at 973 K for 12 h. The prepared catalyst was crushed into monomodal particles of 355–500 μm. For evaluating the surface adsorbate, fine structure, and electric/ionic conduction, a disk was prepared using a pressing apparatus.

Catalyst activity evaluation

For all activity tests, a quartz tube was used as a fixed-bed flow-type reactor. Two electrodes were inserted into the reactor. The electric field was applied using a high-voltage power supply. The catalyst bed temperature was measured using a thermocouple. The imposed current and response voltage were observed using a digital phosphor oscilloscope (Tektronix Inc.). Activity tests were conducted basically at around space velocity of 25 000 h^{-1} at various pre-set temperatures under atmospheric pressure. Reaction rates were estimated in kinetic control. We confirmed that the diffusion is not rate limiting in this condition. Product gases were assessed qualitatively and quantitatively using GC and Q-Mass (QGA; Hiden Analytical Ltd.). Reactant conversion was calculated using the ratio of output moles and input moles. The reaction rate (r) corresponds to the sum of the product flow rates. For reaction with hydrocarbon or CO_2, the carbon deposition amount on the catalyst was evaluated using thermogravimetry with ramping temperature in air.

Characterization

O*perando*-DRIFTS measurements were conducted using FT-IR (Jasco Corp.) with an MCT detector and a diffuse reflectance infrared Fourier transform spectroscopy (DRIFTS) reactor cell (DR-600Ai and DR-600Ci; Jasco Corp.) with a ZnSe window to elucidate the adsorbed species on catalysts with/without the electric field. A DRIFTS cell made of Teflon was used to avoid short circuits in the cell for IR measurements with application of an electric field.

Electrochemical impedance spectroscopy (EIS) measurements for CeO_2 were conducted in a measurement cell (ProboStat; NorECs AS, Norway) with a two-electrode four-wire set up connected to an impedance spectrometer (alpha-A; Novocontrol Technologies) with a ZG4 interface. A schematic illustration of measurement cell is presented in Fig. 4-1. All AC impedance spectra were recorded at frequencies of $10^7 - 10^{-3}$ Hz with amplitude of 0.1 V RMS.

The dispersion of supported active metal was evaluated using CO pulse (BEL CAT II; Microtrac-Bel Japan Inc.). Before

measurements, the catalyst sample was pre-treated under He flow at 473 K for 1 h. After the treatment, the temperature was decreased to 323 K using He. Then 10% CO was pulsed. The TOF-s (based on the metallic surface area) and TOF-p (based on the perimeter of supported metal) were calculated with the number of surface metal atoms and that of interfacial metal atoms, respectively. *Operando* X-ray absorption fine structure (*in-situ* XAFS) spectra were recorded on BL14B2 at SPring-8 (Hyogo, Japan) for evaluation of the fine structure of supported metal and its valence. The crystalline structure was characterized using powder X-ray diffraction (XRD, SmartLab3; Rigaku Corp.) operating at 40 kV and 40 mA with Cu-$K\alpha$ radiation. The structure of supported metal was observed using TEM (JEM-2100F200 kV; JEOL**)**.

Results

Kinetic analyses and isotope effect analyses for various reactions in an electric field

Heterogeneous catalytic reactions in DC electric field have been reported as showing high conversion rates, even at low temperatures of < 500 K. This section presents kinetic evaluation of this phenomenon. The first study is steam reforming of methane over Pd-catalyst supported on CeO_2. Two conditions are applied for this reaction. One is heated by a furnace (SR: steam reforming) controlling the temperature from 423 K to 623 K. Another is with application of DC electric field (ef-SR: electric field assisted steam reforming). The respective temperature dependencies for the reactions (SR and ef-SR) are presented in Fig. 3(A). Under these conditions in the electric field, catalytic activity was very stable. Almost no coke was observed on the Pd/CeO_2 catalyst. Methane conversion increased drastically by the electric field application, even at low temperatures (< 500 K). The activities for ef-SR at low temperatures exceeded the limitation of thermodynamic equilibrium, indicating that the reaction in the electric field includes some irreversible elementary steps. Evaluation was conducted of partial pressure dependencies for both reaction rates. Results show that the dependences of methane pressure were almost first order. The water pressure on the reaction rate was about 0.25 for SR. The trend is similar to those reported from earlier works [48–50]. Actually, ef-SR showed a different trend. The dependence of methane pressure was almost first order. The water pressure was almost zero. To date, many investigations have been conducted for steam reforming of methane. The rate-determining step of methane steam reforming is known to be the methane dissociative adsorption step. For that reason, the partial pressure dependence of methane is almost first-order. However, different trends were observed for ef-SR. The water pressure dependence was greater than that of methane pressure for ef-SR. The application of DC electric field to the heterogeneous catalyst increased the water pressure dependence. Enhancement of the catalytic activity by the electric field is not attributable to Joule heating because the partial pressure dependence of the reaction rate was clearly different, even at the same methane conversion level. Arrhenius plots for both SR and ef-SR are presented in Fig. 3(b), demonstrating that the temperature dependence of reaction

rates with and without the electric field differ considerably. The calculated apparent activation energy was 54 kJ mol^{-1} for SR. On the other hand, the slope of the Arrhenius plot for ef-SR changed at around 600 K. The apparent activation energy decreased to 14 kJ mol^{-1} by application of the electric field at lower reaction temperatures. The reaction mechanism of SR and ef-SR differs markedly, that of ef-SR proceeds along the lower activation energy path at temperatures lower than 600 K.
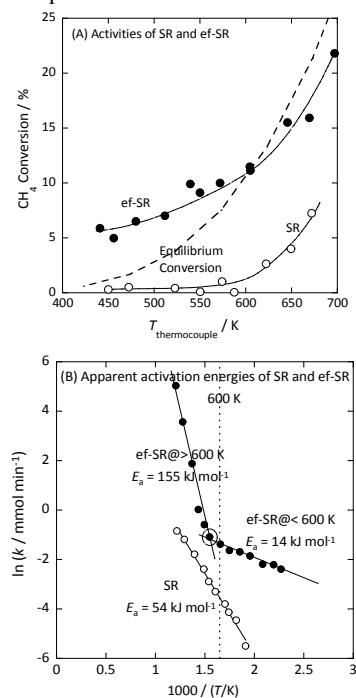

Figure 3 Methane steam reforming activity with (ef-) and without an electric field (A) and apparent activation energy for methane steam reforming with and without an electric field (B) [47].
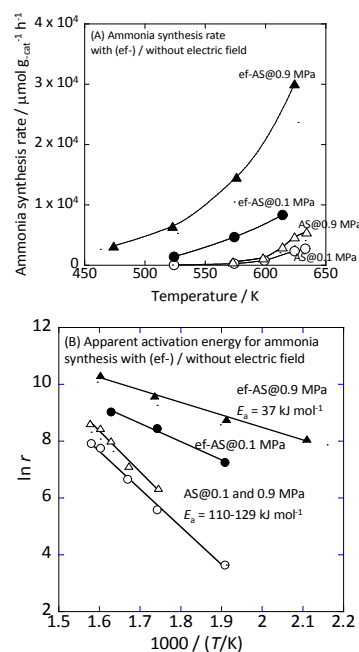

Figure 4 Ammonia synthesis rate with (ef-) and without an electric field (A) and apparent activation energy for ammonia synthesis with and without an electric field (B) [46].

To ascertain of the generality of this phenomenon, we have conducted other reactions in the electric field. This section introduces two other examples: ammonia synthesis and dehydrogenation of methylcyclohexane. Ammonia synthesis (AS) was conducted in the electric field at lower temperatures (denoted as ef-AS) using 9.9wt%Cs/5.0wt%Ru/SrZrO$_3$ catalyst based on our preliminary screening. Fig. 4(A) shows the ammonia synthesis rate with and without the electric field. As observed from this figure, the application of DC electric field enhances the reaction rate drastically. The partial pressure dependence changes by the application of electric field. We obtained a remarkably high ammonia yield, with an ammonia production rate as high as 31 mmol g$_{cat}$$^{-1}$ h^{-1} at 0.9 MPa, which is still in the kinetically controlled region [46]. The activity was stable for a long duration: > 500 hr. The Arrhenius plots for AS and ef-AS are shown in Fig. 4(B). From this figure, a drastic decrease in the apparent activation energy by application of electric field is visible, from 110 kJ mol^{-1} to 37 kJ mol^{-1} by the electric field. For AS (*i.e.* without the electric field), the ammonia synthesis rate exhibited a positive N$_2$ partial pressure dependence of 0.68. The H$_2$ and NH$_3$ partial pressure dependencies were negative: −0.21 for H$_2$ and −0.1 for NH$_3$. These trends coincide with results reported from earlier kinetic studies of ammonia synthesis [51–54]. They indicated that the rate-determining step is N$_2$ activation, especially N$_2$ dissociative adsorption on Ru, because of the strong triple bond of N$_2$ [46]. The negative H$_2$ pressure dependence indicates that the Ru surface was covered by dissociated hydrogen. However, in ef-AS, the N$_2$ and H$_2$ pressure dependencies changed drastically. The N$_2$ pressure dependence was 0.24, which shows that the electric

field promoted the N_2 activation step. Moreover, the H_2 pressure dependence was almost 0: the application of the electric field mitigated the adsorbed hydrogen poisoning of Ru to some degree.

As another example, we conducted dehydrogenation of methylcyclohexane for hydrogen production with and without the electric field over Pt/CeO_2 catalyst. Methylcyclohexane is regarded as a liquid hydrogen carrier. Lowering the dehydrogenation temperature is crucially important. As Fig. 5 shows, the apparent activation energy for the dehydrogenation of methylcyclohexane decreased drastically because of application of the electric field from 56 kJ mol^{-1} to 29 kJ mol^{-1}. These results demonstrate that the application of an electric field to heterogeneous catalyst enables a low-temperature reaction. Therefore, we investigated the reasons why the electric field promoted reactions by isotope exchange tests.
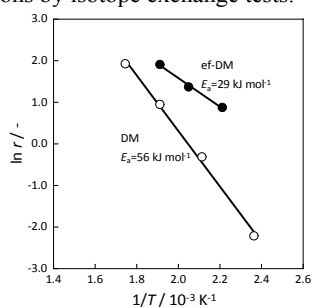

Figure 5 Apparent activation energy for dehydrogenation of methylcyclohexane with (ef-) and without an electric field (B) [41].

Kinetic isotope exchange tests

We conducted kinetic isotope exchange tests using D instead of H on methane steam reforming, ammonia synthesis, and methylcyclohexane dehydrogenation in the electric field. For the procedure, a steady state reaction including H in the reactant was conducted first. Then the flow was switched to another reactant including D at the same temperature. Table 1 presents the H/D isotope exchange tests for these three reactions. As this table shows, the reaction in the electric field showed a higher rate using D instead of H: the "inverse kinetic isotope effect". Generally, a Langmuir–Hinshelwood type surface reaction shows a kinetic isotope effect. Therefore, introduction of D lowers the reaction rate. However, the reaction in the electric field showed higher rates when D was introduced: steam reforming was 1.18 times faster; ammonia synthesis was 1.21 times faster; and methylcyclohexane dehydrogenation was 1.41 times faster. These results correspond to the inverse isotope effect. This fact suggests that the electric field affects changes in the reaction mechanism.

Table 1 Evaluation of kinetic isotope effects on three reactions in the electric field [41, 46, 47]

Reaction	Catalyst	Condition	Reactant	Measured temperature	Reaction rate	k_D/k_H
				/ K	/ mmol h^{-1}	/ -
Methane steam reforming	Pd/CeO$_2$	With electric field	CH$_4$+H$_2$O	473	10.9*	-
			CD$_4$+D$_2$O	473	12.9*	1.18
Ammonia synthesis	Cs/Ru/SrZrO$_2$	With electric field	N$_2$+H$_2$	585	56	-
			N$_2$+D$_2$	588	71.2	1.21
Methyl-cyclohexane dehydrogenation	Pt/CeO$_2$	Without electric field	MCH+H$_2$	519	14.8	-
			MCH$_D$+D$_2$	520	10.2	0.69
		With electric field	MCH+H$_2$	445	8.9	-
			MCH$_D$+D$_2$	442	12.5	1.41

* conversion of methane

***Operando*-DRIFTS measurements**

Considering the adsorption equilibrium, adsorption of molecules on the catalyst surface occurs more readily at lower temperatures. The DC electric field effects on catalytic activity are remarkable at lower temperatures. Therefore, we conducted investigations using *operando*-DRIFTS measurements to evaluate kinetic changes caused by the electric field, based on surface adsorbates. Fig. 6 presents infrared spectra with and without an electric field for steam reforming of methane and for ammonia synthesis.

In case of methane steam reforming (Fig. 6(A)), Pd-catalyst showed many adsorbed species at 473 K in the electric field (not shown). However, the spectrum at 473 K ef-SR over bare CeO$_2$ catalyst showed no adsorbate, indicating that no adsorption enhancement proceeded by application of the electric field without supported Pd. Therefore, Pd supported on CeO$_2$ is regarded as an active site for methane activation in the electric field [47]. Clear differences are visible with and without the electric field from Fig. 6(A). These two reactions, SR at 673 K and ef-SR at 473 K, showed the same methane conversion in this case. This result gives evidence that reaction mechanisms with and without the electric field differ completely. The result also demonstrates that Joule heat is unimportant for reaction in the electric field. The peak assigned to rotation of adsorbed water at 850 cm^{-1} [55] was observed for Pd/CeO$_2$ catalyst only when the electric field was applied at 473 K. This peak is related to the Grotthuss mechanism, a widely known mechanism for proton hopping. On the Grotthuss mechanism, protons hop via adsorbed water molecules with a distorted O–H bond. The rate-determining step of the Grotthuss mechanism is the water rotation step.[55–57] Therefore, activated water exists on the catalyst surface, related to proton hopping. These results reveal that proton hopping occurred via adsorbed water on the catalyst surface during ef-SR.

For ammonia synthesis, application of the electric field brings the formation of peaks at 3146 cm^{-1}, 3046 cm^{-1}, and 2819 cm^{-1}. These peaks were not observed under a pure N_2 supply in

the electric field, or during ammonia synthesis without the electric field even at high temperatures. Therefore, these peaks can be observed only when the electric field was applied to the catalyst bed, and are assigned to the bending and stretching modes of N–H vibrations.[58] In addition, these species remained on the catalyst surface even after stopping of the electric field caused by the strong adsorption of NH_x species on the catalyst.
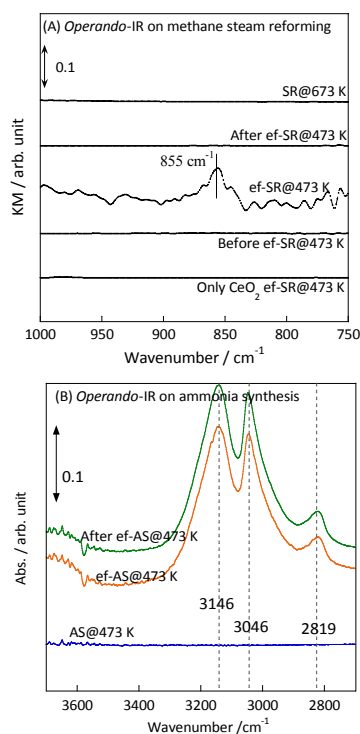

Figure 6 *Operando*-DRIFTS for methane steam reforming (A) and ammonia synthesis (B) with (ef-) and without an electric field [46,47].

Turnover frequency for reactions in the electric field

Considering the role of surface protons, water generally adsorbs on the catalyst support, rather than loaded metal. Hydrocarbons and dinitrogen adsorb on the supported metal particle. Considering this phenomenon, activation of methane, nitrogen, and methylcyclohexane with protons is likely to occur at the metal–support interface. To elucidate the reaction site for both catalyses with and without the DC electric field, we evaluated the turnover frequency by changing the particle size and surface area of the supported metal. Metallic surface area, metal particle size, and the perimeter were evaluated using CO pulse adsorption. Here we defined two turnover frequencies: TOF-s and TOF-p. TOF-s is calculated based on the metallic surface area. TOF-p is calculated based on the perimeter of the supported metal. Fig. 7 presents the trends of two TOFs versus Pd particle size for ef-SR at 473 K and SR at 673 K. Generally, the activity of methane steam reforming is determined by the metallic surface area of supported metal. Regarding SR without the electric field, we obtained the same trends as those reported from the literature, as shown in Fig. 7(b). The TOF-s for SR is the

same despite the Pd metallic surface area. However, these trends differed drastically for ef-SR with the electric field. For these catalysts, the electronic state of the supported Pd was the same, as confirmed by XPS. The ef-SR activity showed strong dependence on the Pd perimeter, rather than on the Pd metallic surface area, which indicates that the ef-SR reaction proceeds mainly at the Pd–CeO$_2$ interface. The same trend was observed for catalytic ammonia synthesis in the electric field, as shown in Fig. 8. From these data, one can infer that ammonia synthesis without an electric field depends on the TOF-s. At around 2 nm particle size of Ru, the B5 site exists, which is known to be highly active for ammonia synthesis. The activity depends on the TOF-p on the reaction in the electric field, as shown in Fig. 8(a), which is evidence that the reaction rate-determining step occurs at the periphery of the supported Ru.
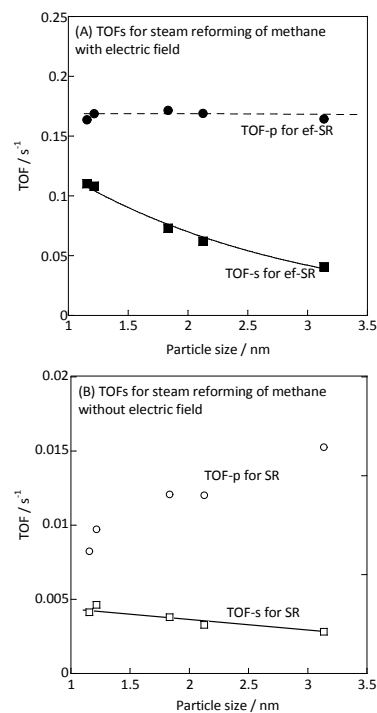

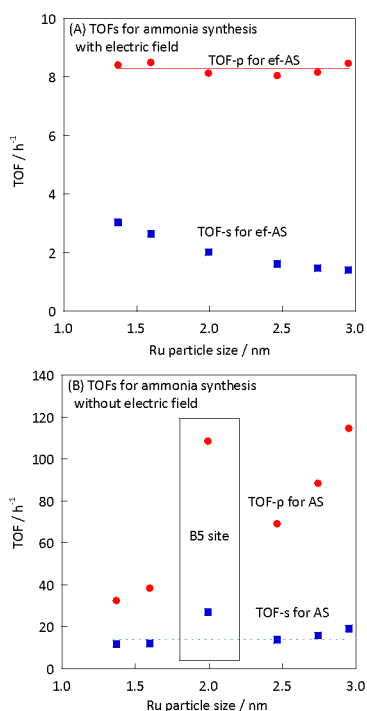Figure 7 Turnover frequencies for methane steam reforming with an electric field (A) and without (B) [47].

Figure 8 Turnover frequencies for ammonia synthesis with electric field (A) and without electric field (B) [46].

Evaluation of surface proton conduction by electrochemical impedance measurements

During the activity test, we observed interesting IV profiles, as shown in Fig. 9. Increasing current lowered the applied voltage, because of control of the current. This result might derive from surface ionic conductivity. For evaluating the surface proton conduction (surface protonics), we conducted electrochemical impedance measurements using catalyst supports used in the kinetic evaluation [59]. Electrochemical impedance measurement is an important method for measuring bulk conductivity. It is used for the evaluation of semiconductors, ion-conductors for fuel cells, batteries, *etc*. We measured the surface conductivity of proton on the catalyst support having higher porosity (*i.e.* low density) for evaluating the surface protonics. For this purpose, we have prepared disc samples of two kinds, with less surface area and with more surface area. Furthermore, we changed the atmosphere to control the surface adsorbate. Nyquist plots are obtained under dry and humid (P_{H2O} = 0.026 atm) conditions by changing the temperatures. In a dry Ar gas atmosphere, two arcs were observed at each temperature. These two arcs are attributable to the resistances of grain bulk (R_b) and grain boundaries (R_{gb}). In a humid atmosphere (P_{H2O} = 0.026 atm), the observed impedance arcs became much smaller by surface ion conduction by the adsorbate on the porous disk. The effect of adsorbate of water vapour on the conductivity is clearer at lower temperatures. The conductivity for surface ionic transport increased from a certain temperature <500 K with lowering of the temperature (Fig. 10). The increased conductivity that occurs with decreasing temperature at constant P_{H2O} is attributable to

increasing surface adsorbate of water for hopping proton via the Grotthuss mechanism.
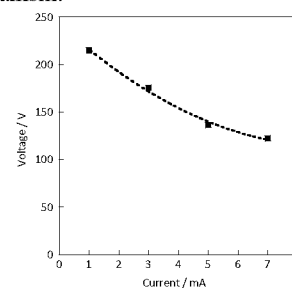

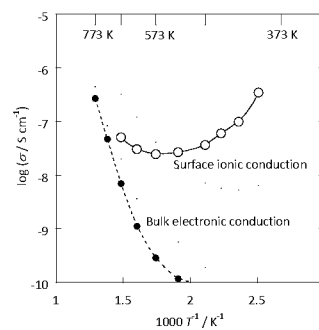Figure 9 IV profile during reaction in the electric field.

Figure 10 Surface ionic conduction and bulk electronic conduction at respective temperatures [59].

We also confirmed the surface protonics in a dry condition with hydrogen gas for porous SrZrO$_3$, the best candidate support for ammonia synthesis in the electric field. By supplying only N$_2$ gas, only two arcs are observed at each temperature. They are attributable to the resistances for grain bulk and the grain boundary. However, by supplying diluted hydrogen, the arcs became much smaller. The effect on conductivity of supplying hydrogen is greater at lower temperatures. For that reason, the surface protonic occurs even in the dry condition with hydrogen. To clarify the dominant carrier on the surface of oxide, isotope tests were conducted using D$_2$ instead of H$_2$. The apparent arcs became larger at 423 K by supplying D$_2$ instead of H$_2$. The ratio of σ_H / σ_D for both surface and interior of SrZrO$_3$ showed higher values of 1.7 and 2.4, indicating that proton diffuses both in the bulk of SrZrO$_3$ and on the surface of SrZrO$_3$ at lower temperatures.
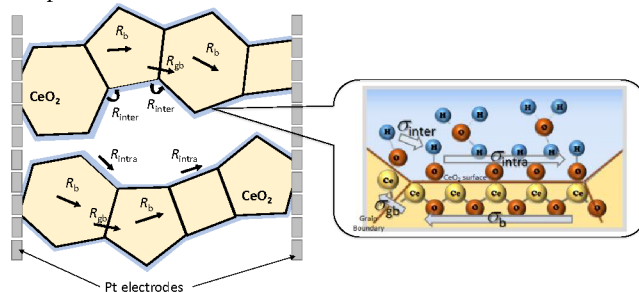

Figure 11 Mechanism and image of surface proton hopping [59].

Surface proton transport properties for catalyst support under humid and dry conditions were investigated using electrochemical impedance spectroscopy. Using samples of low relative density at 60% enables evaluation of the interior and surface conductivities. The surface protonic conductivity under humid and dry conditions increased concomitantly with decreasing temperatures, indicating that adsorbed water or hydrogen plays an important role for proton hopping on the catalyst surface. A related schematic image is shown in Fig. 11.

Discussion

Our experimentally obtained results indicate that surface proton hopping (surface protonics) plays an important role in various heterogeneous catalyses, including those of methane steam reforming, ammonia synthesis, and dehydrogenation of methylcyclohexane. Proton conduction is known to play an important role in fuel cells, electrolysers, gas-separation membranes, sensors, and catalysis. Therefore, numerous investigations have already been conducted to assess solid-state protonic conduction. Regarding proton conductivity, the proton concentration and mobility are fundamentally important for achieving high protonic conductivity. Regarding mobility, ionic mobility including that of protons is regarded as linked with the Nernst–Einstein relation, as presented in equation (1), where D is the diffusion coefficient, R is the gas constant, z stands for the electric charge, and F is the Faraday constant.

$D = \mu RT/zF$ 　　　　　　　　　eq. 1

The diffusion coefficient follows Arrhenius behaviour. Therefore, the proton mobility can be expressed as Arrhenius-type, as in equation (2). Thereby, the ionic conductivity can be discussed as a function of inverse temperature, as shown in equation (3).

$\mu = \mu_0\, 1/T \exp((-\Delta H)/RT)$ 　　　　eq. 2

$\sigma = \sigma_0 \exp((-\Delta E)/RT)$ or $\sigma_0\, 1/T \exp((-\Delta E)/RT)$ 　　eq. 3

With respect to the mechanism of proton conduction, two main mechanisms are known to exist for proton conductivity. One is that by which a proton itself diffuses toward the nearest O–H species through hydrogen bonding: the so-called *Grotthuss* mechanism.[60] The other is that by which a proton diffuses as a hydrated ion: the so-called vehicle mechanism.[61] A schematic illustration of mechanisms for proton conductivity is portrayed in Fig. 12. The activation energy for *Grotthuss* mechanism is reported as smaller values of below 0.5 eV than those for a vehicle mechanism below 1.0 eV.[62]
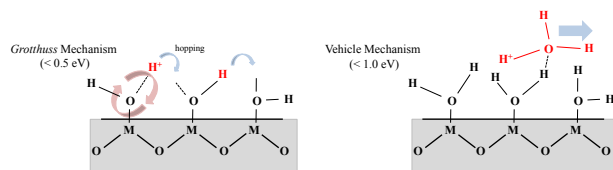

Figure 12 Schematic illustrations of proton conductivity mechanisms.

Numerous materials have been reported as proton conductors. Among them, solid-state protonic conductors are often classified in terms of the transported species, the type of synthesis for materials, operating temperature range, organic or inorganic compounds, and so on [63]. Generally speaking, there are two ways to generate protons from supplied water vapour. Protons can be generated from interaction between water vapour and oxygen vacancy [64], as shown in equation (4). Alternatively, protons can be generated as derived from acid–base properties of solid oxides [65], as in equation (5), where M denotes the adsorbed sites for water.

$H_2O + O^x_o + V^{\cdot\cdot}_o = 2OH^\cdot_o,$ 　　　　eq. 4

$M\text{-}OH + M\text{-}OH \rightarrow M\text{-}O^- + M\text{-}OH_2^+$ 　　eq. 5

Regarding the former point, the reaction of equation (4) is generally exothermic, such that low temperatures are favourable for proton production. High temperatures are favourable for the formation of oxygen vacancies. Therefore, many researchers have devoted attention to acceptor doping to increase the proton concentration.[66–72] Yttrium, barium, gadolinium, and strontium are the candidates of dopant for achieving high proton conductivity toward $BaCeO_3$ [66,67], $Ba_2YSnO_{5.5}$ [68], $BaZrO_3$ [69] and perovskite-structure materials such as $LaErO_3$ [70], $LaPO_4$ [71], and $BaPrO_3$ [72].

In contrast to ionic conduction of interior solid electrolytes, proton conduction via adsorbed water onto oxides, so-called "surface protonics", has been investigated, especially since 2010. Researchers used Y-stabilized ZrO_2 (YSZ) [73,74], TiO_2 [75], and CeO_2-based oxides [76] as examples of nanocrystalline oxides. Peculiar dependence of surface conductivity was observed on YSZ [73] below 500 K. At lower temperatures, water adsorption onto the oxides is favourable.[72] Therefore, we might conclude that a layer of adsorbed water forms hydrogen bonding, yielding high protonic conductivity at low temperatures. It contributes to the surface heterogeneous catalysis in the DC electric field.

Conclusion

A catalytic reaction mechanism in an electric field is completely different from conventional catalytic reactions, as evidenced by kinetic evaluation including the Arrhenius plot and partial pressure dependence, *operando*-IR, and kinetic isotope effect. Considering these phenomena, the reaction mechanism in the electric field can be regarded explained below. First, proton forms on the catalyst support surface from water or hydrogen adsorbate. After the formed surface proton is driven by the electric field application, it collides with adsorbed reactant (*e.g.*. methane, nitrogen, methylcyclohexane) at the periphery of the supported metal. Then activated intermediate (C-H-H+, N-N-H+, *etc.*) is formed. It is converted to products on the metal particle surface. C-H dissociation or nitrogen dissociation, which are the rate-determining steps over ordinary heterogeneous catalyst, is promoted by the formation of such an intermediate (C-H-H+, N-N-H+, *etc.*) by the electric field. For the case of ammonia synthesis, the mechanism through N_2H^+ brings higher reactivity for dissociating strong nitrogen triple bonds. Theoretical DFT calculations also lead to results that agree with those of the

ARTICLE

assumed model. High protonic conductivity on the catalyst support enhances the catalytic activity.

Conflict of interest

The authors have no conflict to declare.

Acknowledgements

Notes and references

1   S. Kado, Y. Sekine and K. Fujimoto, *Chem. Commun.* 1999, **24**, 2485-2486.
2   S. Kado, K. Urasaki, Y. Sekine and K. Fujimoto, *Chem. Commun.* 2001, 415-416.
3   M. Kraus, B. Eliasson, U. Kogelschatz and A. Wokaun, *Phys. Chem. Chem. Phys.* 2001, **3**, 294-300.
4   T. Jiang, Y. Li, C. Liu, G. Xu, B. Eliasson and B. Xue, *Catal. Today* 2002, **72**, 229-235.
5   S. Kado, K. Urasaki, Y. Sekine and K. Fujimoto, *Fuel* 2003, **82**, 1377-1385.
6   Y. Sekine, K. Urasaki, S. Kado, M. Matsukata and E. Kikuchi, *Energy Fuels* 2004, **18**, 455-459.
7   Y. Sekine, K. Urasaki, S. Asai, M. Matsukata, E. Kikuchi and S. Kado, *Chem. Commun.* 2005, 78-79.
8   Y. Sekine, J. Yamadera, S. Kado, M. Matsukata and E. Kikuchi, *Energy Fuels* 2008, **22**, 693-694.
9   C. Liu, A. Marafee, B. Hill, G. Xu, R. Mallinson and L. Lobban, *Ind. Eng. Chem. Res.* 1996, **35**, 3295-3301.
10 C. Liu, A. Marafee, R. Mallinson and L. Lobban, *Appl. Catal. A. Gen.* 1997, **164**, 21-33.
11 A. Marafee, C. Liu, G. Xu, R. Mallinson and L. Lobban, *Ind. Eng. Chem. Res.* 1997, **36**, 632-637.
12 M. Stoukides and C. G. Vayenas, *J. Catal.* 1981, **70**, 137-146.
13 C. G. Vayenas, S. Bebelis and S. Neophytides, *J. Phys. Chem.* 1988, **92**, 5083-5085.
14 J. Pritchard, *Nature* 1990, **343**, 592-593.
15 A. Katsaounis, *J. Appl. Electrochem.* 2010, **40**, 885-902.
16 I. V. Yentekakis, Y. Jiang S. Neophytides, S. Bebelis and C. G. Vayenas, *Ionics* 1995, **1,** 491-498.
17 A. de Lucas-Consuegra, A. Caravaca, P. J. Martinez, J. L. Endrino, F. Dorado and J. L. Valverde, *J. Catal.* 2010, **274**, 251-258.
18 A. Caravaca, A. de Lucas-Consuegra, C. Molina-Mora, J. L. Valverde and F. Dorado, *Appl. Catal. B. Environ.* 2011, **106**, 54-62.
19 C. Jimenez-Borja, F. Dorado, A. de Lucas-Consuegra, J. M. Garcia-Vargas and J. L. Valverde, *Catal. Today* 2009, **146**, 326-329.
20 M. Ouzounidou, A. Skodra, C. Kokkohitis and M. Stoukides, *Solid State Ionics* 2007, **178**, 153-159.
21 C. G. Yiokari, G. E. Pitselis, D. G. Polydoros, A. D. Katsounis and C. G. Vayenas, *J. Phys. Chem. A* 2000, **104**, 10600-10602.
22 G. Marnellos, S. Zisekas and M. Stoukides, *J. Catal.* 2000, **193**, 80-87.
23 V. Kiriyakou, C. Athanasiou, I. Garagounis, A. Skodra and M. Stoukides, *Int. J. Hydrogen Energy* 2012, **37**, 16636-16641.
24 C. G. Vayenas, S. Bebelis and S. Ladas, *Nature* 1990, **343**, 625.
25 J. R. Rostrup-Nielsen, *J. Catal.* 1973, **31**, 173-199.
26 A. Mittasch and W. Frankenburg, *Adv. Catal.* 1950, **2**, 81-104.
27 G. Ertl, *Catal. Rev. Sci. Eng.* 1980, **21**, 201-223.
28 K. Aika, H. Hori and A. Ozaki, *J. Catal.* 1972, **27**, 424-431.

29 Y. Sekine, M. Haraguchi, M. Tomioka, M. Matsukata and E. Kikuchi, *J. Phys. Chem. A* 2010, **114**, 3824-3833.
30 Y. Sekine, M. Tomioka, M. Matsukata and E. Kikuchi, *Catal. Today* 2009, **146**, 183-187.
31 Y. Sekine, M. Haraguchi, M. Matsukata and E. Kikuchi, *Catal. Today* 2011, **171**, 116-125.
32 K. Oshima, T. Shinagawa, M. Haraguchi and Y. Sekine, *Int. J. Hydrogen Energy* 2013, **38**, 3003-3011.
33 K. Oshima, T. Shinagawa, Y. Nogami, R. Manabe, S. Ogo and Y. Sekine, *Catal. Today* 2014, **232**, 27-32.
34 Y. Sekine, K. Yamagishi, Y. Nogami, R. Manabe, K. Oshima and S. Ogo, *Catal. Lett.* 2016, **146**, 1423-1428.
35 T. Yabe, K. Mitarai, K. Oshima, S. Ogo and Y. Sekine, *Fuel Process. Technol.* 2017, **158**, 96-103.
36 S. Ogo and Y. Sekine, *Chem. Record* 2017, **17**, 726-738.
37 M. Torimoto, K. Murakami and Y. Sekine, *Bull. Chem. Soc. Jpn.* 2019, **92**(10), 1785-1792.
38 M. Torimoto, S. Ogo, D. Harjowinoto, T. Higo, J-G. Seo, S. Furukawa and Y. Sekine, *Chem. Commun.* 2019, **55**, 6693-6695.
39 T. Yabe, K. Yamada, K. Murakami, K. Toko, K. Ito, T. Higo, S. Ogo and Y. Sekine, *ACS Sustain. Chem. Eng.* 2019, **7**(6), 5690-5697.
40 K. Takise, A. Sato, K. Muraguchi, S. Ogo and Y. Sekine, *Appl. Catal. A: Gen.* 2019, **573**, 56-63.
41 K. Takise, A. Sato, K. Murakami, S. Ogo, J-G. Seo, K. Imagawa, S. Kado and Y. Sekine, *RSC Adv.* 2019, **9**, 5918-5924.
42 K. Takise, A. Sato, S. Ogo, J-G. Seo, K. Imagawa, S. Kado and Y. Sekine, *RSC Adv.* 2019, **9**, 27743-27748.
43 M. Kosaka, T. Higo, S. Ogo, J-G. Seo, K. Imagawa, S. Kado and Y. Sekine, *Int. J. Hydrogen Energy*, in press. doi: 10.1016/j.ijhydene.2019.10.133
44 T. Yabe, K. Yamada, T. Oguri, T. Higo, S. Ogo and Y. Sekine, *ACS Catal.* 2018, **8**, 11470-11477.
45 R. Inagaki, R. Manabe, Y. Hisai, Y. Kamite, T. Yabe, S. Ogo and Y. Sekine, *Int. J. Hydrogen Energy* 2018, **43**(31), 14310-14318.
46 R. Manabe, H. Nakatsubo, A. Gondo, K. Murakami, S. Ogo, H. Tsuneki, M. Ikeda, A. Ishikawa, H. Nakai and Y. Sekine, *Chem. Sci.* 2017, **8**, 5434-5439.
47 R. Manabe, S. Okada, R. Inagaki, K. Oshima, S. Ogo and Y. Sekine, *Sci. Rep.* 2016, **6**, 38007.
48 J. Wei and E. Iglesia, *J. Catal.* 2004, **225**, 116–127.
49 J. Wei and E. Iglesia, *J. Catal.* 2004, **224**, 370–383.
50 A. Yamaguchi and E. Iglesia, *J. Catal.* 2010, **274**, 52–63.
51 F. Rosowski, A. Hornung, O. Hinrichsen, D. Herein, M. Muhler and G. Ertl, *Appl. Catal. A: Gen.* 1997, **151**, 443–460.
52 H. Bielawa, O. Hinrichsen, A. Birkner and M. Muhler, *Angew. Chem. Int. Ed.* 2001, **40**, 1061–1063.
53 K. Aika, M. Kumasaka, T. Oma, O. Kato, H. Matsuda, N. Watanabe, K. Yamazaki, A. Ozaki and T. Onishi, *Appl. Catal.* 1986, **28**, 57–68.
54 S. Hagen, R. Barfod, R. Fehrmann, C. J. Jacobsen, H. T. Teunissen and L. B. Chorkendorff, *J. Catal.* 2003, **214**, 327–335.
55 S. Ashihara, *The Molecular Simulation Society of Japan* 2009, **11**(2), 20–24.
56 M. Eikerling and A. Kornyshev, *J. Electroanal. Chem.* 2001, **502**, 1–14.
57 T. Erdy-Gruz and S. Lengyel, *Modern Aspects of Electrochemistry* 1977, **12**, 1–40.
58 E. L. Wagner and D. F. Hornig, *J. Phys. Chem.* 1950, **18**, 296–303.
59 R. Manabe, S. Stub, T. Norby, and Y. Sekine, *Solid State Commun.* 2018, **270**, 45-49.
60 N. Agmon, *Chem. Phys. Lett.* 1995, **244**, 456–462.

61 K. D. Kreuer, A. Rabenau and W. Weppner, *Angew. Chem.* 1982, **21**, 208–209.
62 K. D. Kreuer, *Solid State Ionics* 2000, **136–137**, 149–160.
63 T. Norby, *Solid State Ionics* 1999, **125**, 1–11.9.
64 T. Norby, *MRS Bulletin* 2009, **34**, 923–928.
65 J. H. Anderson and G. A. Parks, *J. Phys. Chem.* 1968, **72**, 3662–3667.
66 K. D. Kreuer, T. Dippel, Y. M. Baikov and J. Maier, *Solid State Ionics* 1996, **86–88**, 613–620.
67 T. Norby and Y. Larring, *Solid State Mater. Sci.* 1997, **2**, 593–599.
68 K. D. Kreuer, *Solid State Ionics* 1997, **97**, 1–15.
69 K. D. Kreuer, *Solid State Ionics* 1999, **125**, 285–302.
70 Y. Larring and T. Norby, *Solid State Ionics* 1994, **70–71**, 305–310.
71 T. Norby and N. Christiansen, *Solid State Ionics* 1995, **77**, 240–243.
72 T. Fukui, S. Ohara and S. Kawatsu, *J. Power Sources* 1998, **71**, 164–168.
73 S. Miyoshi, Y. Akao, N. Kuwata, J. Kawamura, Y. Oyama T. Yagi and S. Yamaguchi, *Chem. Mater.* 2014, **26**, 5194–5200.
74 S. Ø. Stub, E. Vøllestad and T. Norby, *J. Phys. Chem. C* 2017, **121**, 12817–12825.
75 I. G. Tredici, F. Maglia, C. Ferrara, P. Mustarelli and U. Anselmi-Tamburini, *Adv. Funct. Mater.* 2014, **24**, 5137–5146.
76 M. Shirpour, G. Gregori, R. Merkle and J. Maier, *Phys. Chem. Chem. Phys.* 2011, **13**, 937–940.